THERMO-CHEMISTRY OF NON-METALLIC INCLUSIONS IN DUCTILE IRON

S. Lekakh, V. Richards, and K. Peaslee
Missouri University of Science and Technology, Rolla, MO, USA

Abstract

Non-metallic inclusions formed during multi-stage ductile iron melt treatment play an important role in solidification, structure, and casting quality. Professor Carl Loper made fundamental studies on the role of inclusions in heterogeneous nucleation of graphite. In this article, a comparison of inclusions in steel and cast iron was done using thermodynamic calculations (FACTSAGE software) and automated SEM/EDS inclusion analysis (ASPEX system). Statistics of non-metallic inclusions (size, shape, composition) were studied in the iron and steel samples collected by quenching after different stages of melt treatment as well as from castings. The suggested methodology of inclusion analysis has the potential to be applied together with adaptive thermal analysis (ATAS) for solving practical problems such as decreasing shrinkage defects in ductile iron.

Keywords: *inclusions, ductile iron, spheroidal graphite, flake, nucleation*

Introduction

This article was specially written for the Carl Loper Cast Iron Symposium. Professor Loper has been doing research and industrial development in metal casting during the last five decades. His scientific interests cover the spectrum of different cast alloys with some of his most significant contributions achieved in the areas of: cast iron, casting solidification, ductile iron (DI), and inoculation. Table 1 presents the number of his published and refereed articles according to Cambridge Scientific Abstract and METADEX databases, an indication of his prolific writing abilities, outstanding record of contribution and the high regard of that contribution in the industrial and scientific communities.

DI treatment dramatically changes the structure and the properties of castings. Deep refining of the melt by *Mg* transforms the flake graphite to spheroidal graphite. Because liquid iron treated by magnesium has a tendency to undercool resulting in meta-stable cementite formation, DI treatment also includes inoculation by *FeSi(X)(where X is Al, Ca, Ba, Sr)* additives which create additional graphite nuclei, resulting in a carbide-free structure even in thin wall castings. Therefore, the industrial DI treatment typically consists of two stages – nodulization and inoculation. These processes were studied by C. Loper and coauthors[1-4] as well as other authors[5-7] from different perspectives. In this article, computational-thermodynamic and experimental methods were used to study refining reactions in liquid iron and steel. Non-metallic inclusions formed during these refining reactions can influence heterogeneous graphite nucleation. This paper introduces a method to statistically evaluate the inclusion population in DI, a novel application of the automated inclusion analyzer.

Procedure

Traditional thermodynamics can be used to determine the equilibrium conditions of separate individual reactions and is often used for analysis of the refining processes in cast irons. However, in actual liquid metal processing parallel reactions take place. The same additive can react with more than one impurity and, at the same time, one impurity can interact with different active additives**.** The possible changes in the melt composition from the initial stage to the equilibrium state are critical in many practical cases**.** To get around these problems, computer simulation, based on the minimization of the Gibbs free energy, was applied. This

Table 1. Published and refereed articles of Dr. Loper according Cambridge Scientific Abstract and METADEX

Topic	Cambridge Scientific Abstract (METADEX)	
	Published	Refereed
Cast iron	200 (182)	313 (285)
Solidification	111 (93)	208 (174)
Ductile iron	65 (62)	122 (118)
Inoculation	33 (33)	53 (53)

allowed the parallel reactions to be simulated step-by step as the amount of additive was increased. Simulations of the reactions of nodulizing and inoculation additives were carried out using FACTSAGE for the complex additive compositions and the amounts which are used in industrial practice.

For experimental verification of computed refining reactions, specimens of iron-carbon-silicon (3.7 wt.% *C*, 1.8 wt.% *Si*) alloys were prepared from pure (99.99 wt.%) charge materials held in alumina crucibles (200 gram size) in a furnace having silicon carbide heating elements under an argon atmosphere. These alloys contained two levels of sulfur content, the first one was a relatively pure alloy with less than 0.005 wt.% *S* and the second alloy had 0.04 wt.% *S*. The master alloys used for refining the iron melts were *Cu*-15 wt.% *Ca*, *Fe*-50 wt.% *Ce*, and *Ni*-10 wt.% *Mg*. After the liquid iron treatment, the oxygen activity was measured using a solid electrolyte (zirconium oxide stabilized by yttrium oxide) probe with $Mo\text{-}MoO_2$ reference electrode.

In addition, DI heats were melted in a 100 lb induction furnace using pig iron and steel stampings. A two step DI treatment included pre-treatment by submerging 0.1 wt. % *Ca-La* mishmetal in the induction furnace followed by 1.8 wt.% nodulizer (*Fe*-6%wt.%*Mg*-55 wt.%*Si)* and 0.2% inoculant (*Fe*-75wt.%*Si*) in the ladle. Samples were collected directly from the melt using submerged core samplers with two internal chill plates as well as from the 20 mm (2 cm) casting wall.

The total oxygen content, which is present either dissolved in the matrix as "free" oxygen or as oxygen in inclusions, was measured using a Leco TC-500 analyzer. Non-metallic inclusions were studied using an automated inclusion analyzer system, the Aspex PICA-1020. The automated inclusion analysis is described elsewhere.[8] Briefly, in the Aspex SEM system, a focused electron beam is moved across the specimen in an array of fairly coarse steps, as shown in Fig. 1a. The field is subdivided into smaller fields (Fig. 1b). As the electron beam moves across each field, the brightness or intensity of the back scattered electron detector (BSED) signal is recorded. If the signal is bright (or dark) enough to indicate that an inclusion is present at the position, the software initiates a particle-sizing sequence using a rotating chord algorithm (Fig. 1c). This is a fast process because the instrument only spends time collecting detailed EDS data where inclusions are known to be present. Subsequently, number, size, and shape parameters are computed from the lengths of the chords. After the sample is completely analyzed, the data is evaluated using automated feature analysis software. The inclusions were classified into various classes based on their composition as determined by user-defined rules.

Thermodynamics of Refining Reactions in Liquid Steel Versus Iron

Calcium

In liquid low carbon steel at 1600C (1873K), the calculated sequence of reactions of *Ca* additions with sulfur and oxygen are depicted in Fig. 2a. Small additions of calcium react first with oxygen, and only after the addition of larger amounts of calcium will it react with sulfur. The amount of calcium required for deep refining depends on the initial *[O]* and *[S]* contents in the steel melt. In the case of liquid cast iron (3.7 wt.% *C* and 1.8 wt.% *Si* at 1400C [1673K]), *Si* and *C* change the sulfur and oxygen activities and so the sequence of their reactions with *Ca* is reversed (Fig. 2b). The extent of deoxidization is limited by the CaC_2 formation in the liquid cast iron. Solid, dashed and dotted lines show the calculated interactions of *Ca* for the different initial concentrations of impurities in the melts.

The oxygen activities $a_{[O]}$ following *Ca* additions in the liquid cast iron having different initial sulfur contents were measured for experimental confirmation of the cal-

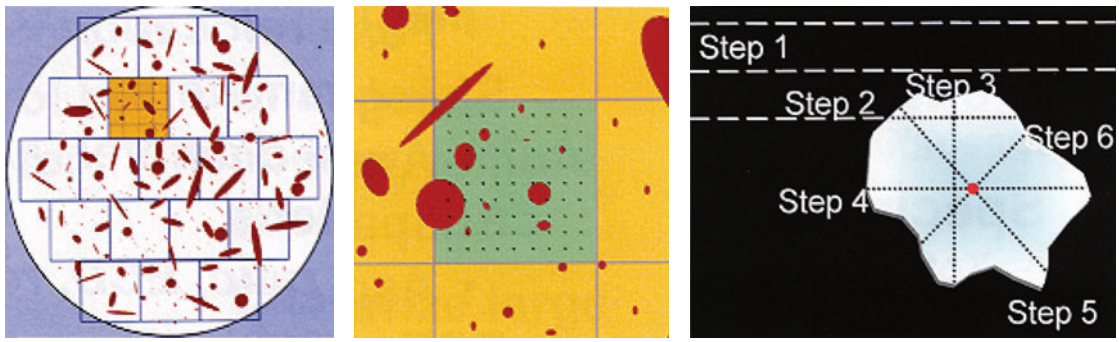

(a) *(b)* *(c)*

Figure 1. Automated inclusion analysis including (a) subdividing the image into fields, (b) moving electron beam across field in an array and (c) sizing and cataloging of particles detected by back scattering electrons and centering the beam on each particle and obtaining composition by x-ray spectroscopy.[8]

culated sequences of the refining reactions (Fig. 3). The increase of *Ca* additives was proportional to the decrease in the oxygen activities in the high purity *Fe-C-Si* irons melted in an argon atmosphere. While the initial melt contained 0.04 wt.% *S*, there was a negligible influence of small *Ca* additives on $a_{[O].}$ The oxygen activity in the melt decreased only after desulfurization with larger amounts of the calcium additives. At the same time, an oxygen activity smaller than $1x10^{-4}$ was not reached. The shape of flake graphite in the cast iron treated by calcium did not change. These experiments confirmed the calculated prediction of the sequences of the refining reactions of *Ca* in the liquid cast iron.

Magnesium

The calculated data showed that a small amount of added magnesium (Mg^a) produced significant deoxidation of the cast iron melts with different initial *S* levels (Fig. 4a). The two parallel refining reactions took place when Mg^a was increased. Unlike *Ca*, the Mg^a reaction with oxygen in the liquid cast iron is not limited by carbide formation. It is generally accepted that 0.02 - 0.03 wt.% free (dissolved in the melt) Mg^f is necessary for transformation of the flake graphite to spherical graphite. The oxygen $[O]^{DI}$ in equilibrium with this Mg^f is shown in Fig. 4b by a dashed line. This calculated sequence of the reactions in the magnesium treated cast irons was experimentally confirmed (Fig. 4b). A small amount of Mg^a dramatically decreased a_O in all irons while the reaction with *[S]* forced deoxidation to occur later in the cast irons having larger initial sulfur contents. The remaining concentration of *[S]* and a_O decreased at the same time. After that, when Mg^a was sufficient to react with *[S]* and decrease the a_O to a value less than $8x10^{-5}$ wt.%, the flake shape of graphite transformed to the spherical shape. The correlation between the measured $[Mg^f]$ and a_O in the melts, and the resulting graphite structure is shown in Fig. 5.

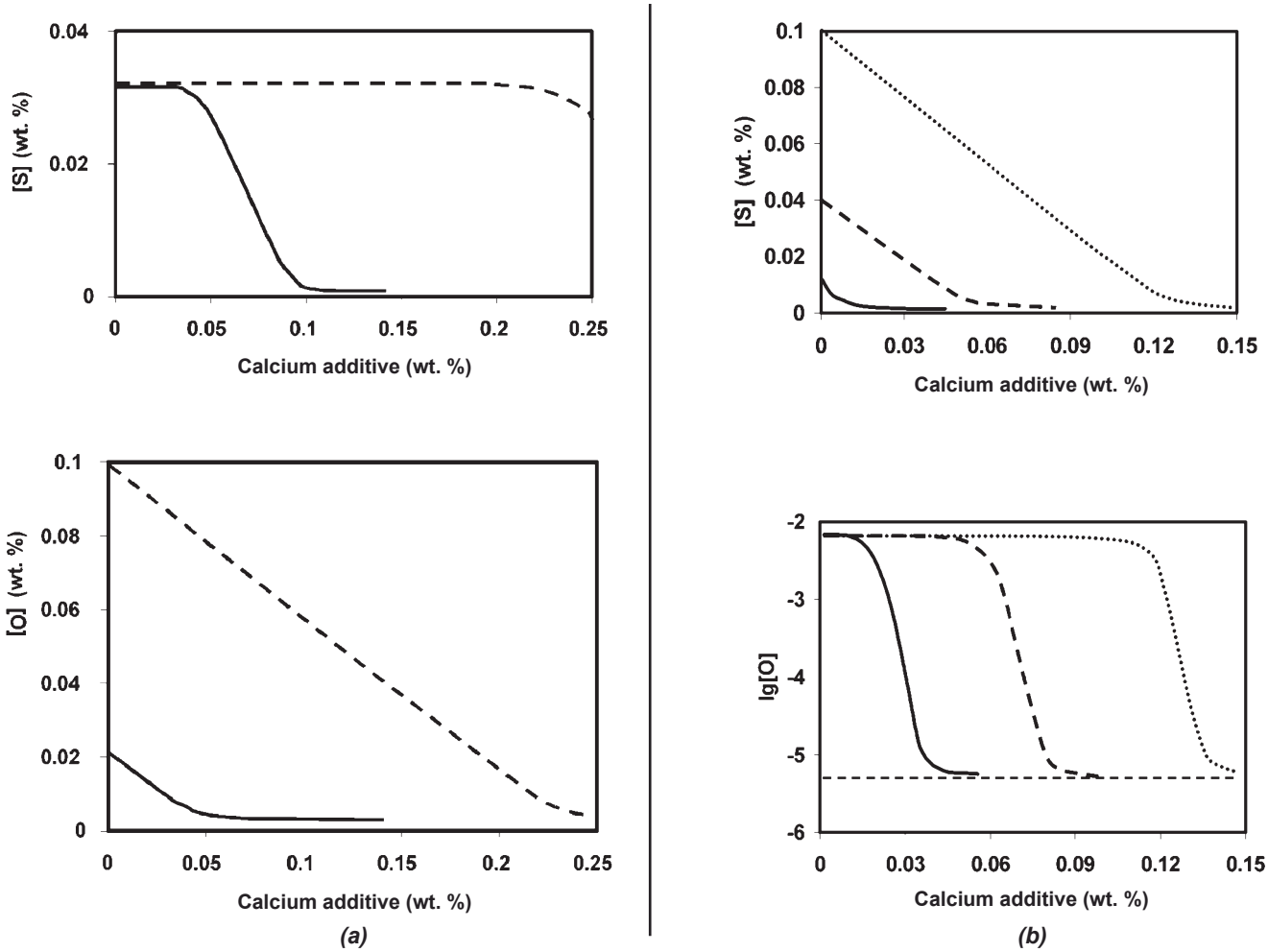

Figure 2. (a) The calculated interactions of the Ca with [S] and [O] in steel at 1873K and (b) in cast iron at 1673K.

Cerium and Complex Additives

Cerium in cast iron melts *[Ce]* has thermodynamic properties between *[Ca]* and *[Mg]* and can create sulfides (*CeS*, Ce_2S_3), oxides (Ce_2O_3) and more complicated oxy-sulfide compounds (Ce_2O_2S). Calculations predict that Ce^a could react simultaneously with *[O]* and *[S]*. Measurement of a_O showed, that Ce^a simultaneously reduced a_O and the final concentration of sulfur in the melt confirming the computer simulations. The sequence of refining reactions in liquid steel and iron treated by *Ca, Mg* or *Ce* is schematically illustrated in Fig. 6. The shaded areas refer to the amount of each additive used for reaction with the impurities *[S]* and *[O]* in the melts. Alkali and rare earth metals first deeply deoxidize liquid steel and then further additions produce desulfurization. But in the liquid cast irons, alkali and rare earth metals have different sequences of refining reactions, which depend not only on the additive type and composition, but also on the composition of the initial melt.

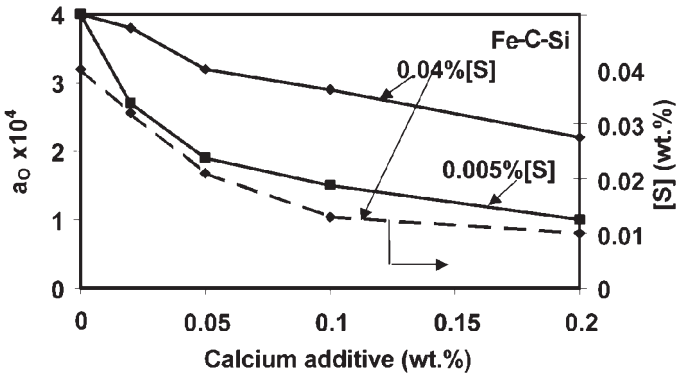

Figure 3. Influence of Ca addition on $a_{[O]}$ and final sulfur contents in Fe-C-Si alloys with different initial sulfur contents.

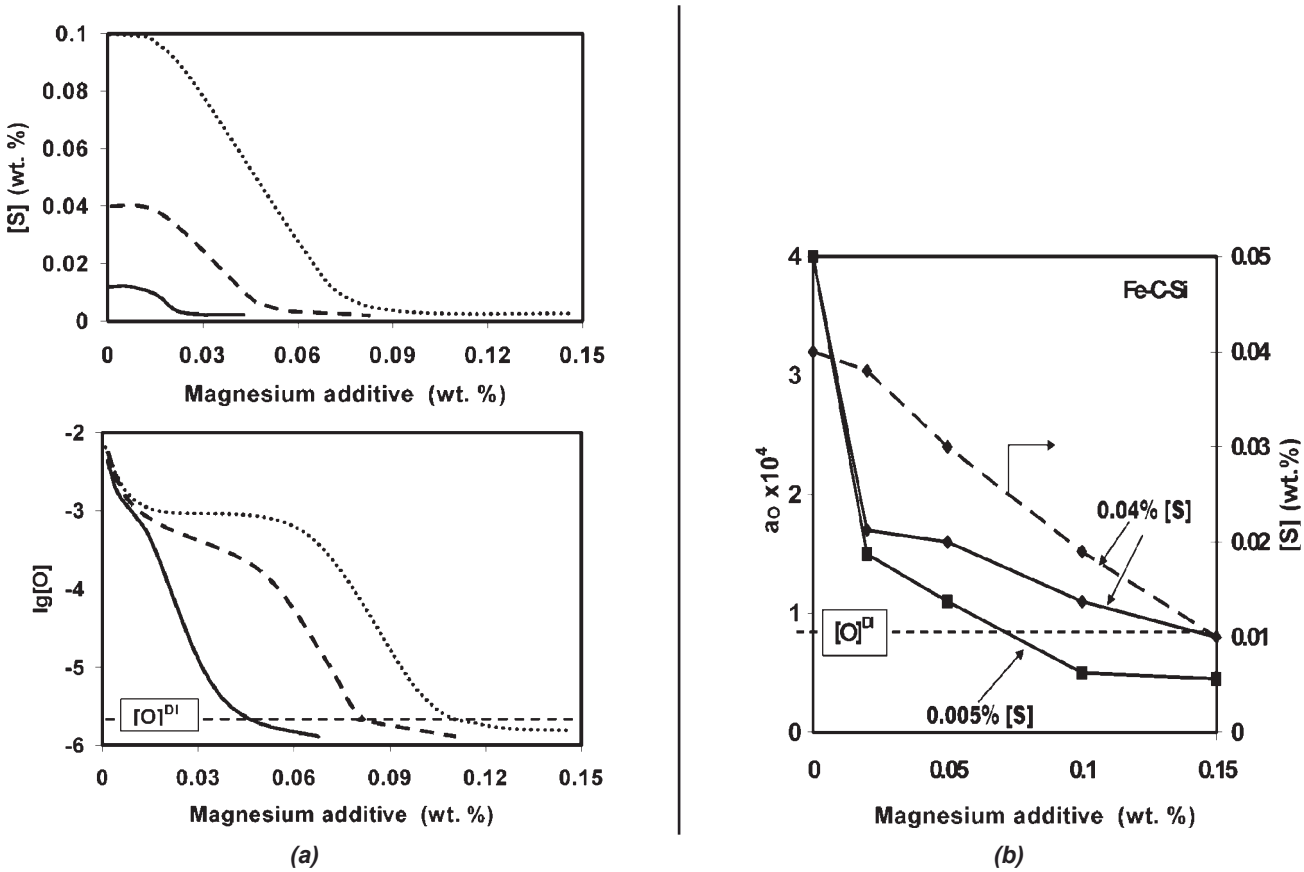

Figure 4. The reactions of Mg^a in alloys with different initial sulfur contents: (a) calculated reactions in cast iron at 1673K, and (b) measured $a_{[O]}$ and final sulfur contents in Fe-C-Si alloys.

The individual features of the reactive species can be exploited in the design of complex refining additives to be used, for example, to increase the effectiveness of ductile iron treatment. An example of a calculated 3-D diagram which describes the complex interaction of Mg^a and Ca^a additives with impurities *[S]* and *[O]* in the iron melt is given in Fig. 7. The regions indicating the reactions of Mg^a with *[O]* and *[S]* are designated as $[Mg]^O$ and $[Mg]^S$ respectively. Excess Mg^a creates free magnesium in the melt $[Mg]^f$ the quantity of which depends on calcium additives Ca^a. If complex *Mg* and *Ca* additives are used, the refining functions are divided between these elements. Most of Ca^a is consumed in the reaction with *[S]*, while Mg^a reacts with *[O]*. It is important to note that calcium can decrease the critical values of the total magnesium added, which is necessary for ductile iron nodulizing treatment.

Non-Metallic Inclusions in Steel Treated by *Ca* Wire

Samples were collected[9] from the different processing steps of melting steel in a 20t acid lined electric arc furnace and from the ladle before and after Ca-wire treatment as well as from the final casting (Fig. 8). The volume of inclusions decreased after addition of the *Ca* due to the formation of calcium aluminates (*CA*). Also in this process, *MnS* inclusions were modified to *CaS*. These transformations are illustrated in Fig. 9 and mapping of inclusion chemistry is showing in Fig. 10. *Ca*-wire treatment in the 20t ladle provides high and

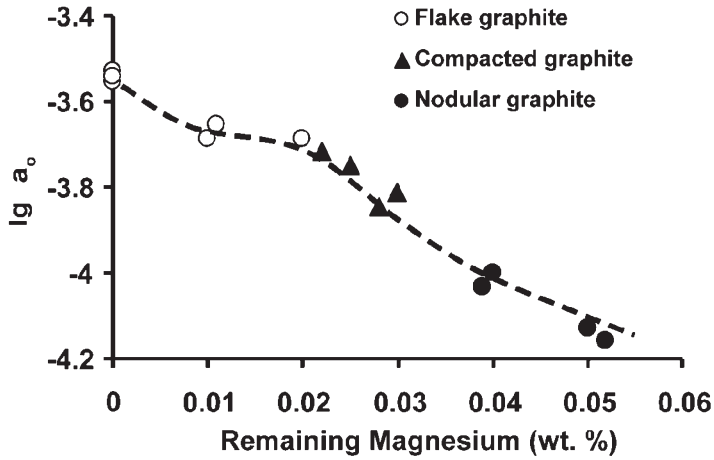

Figure 5. Correlation of a_o with $[Mg^f]$ in the melt and shape of graphite in solid irons.

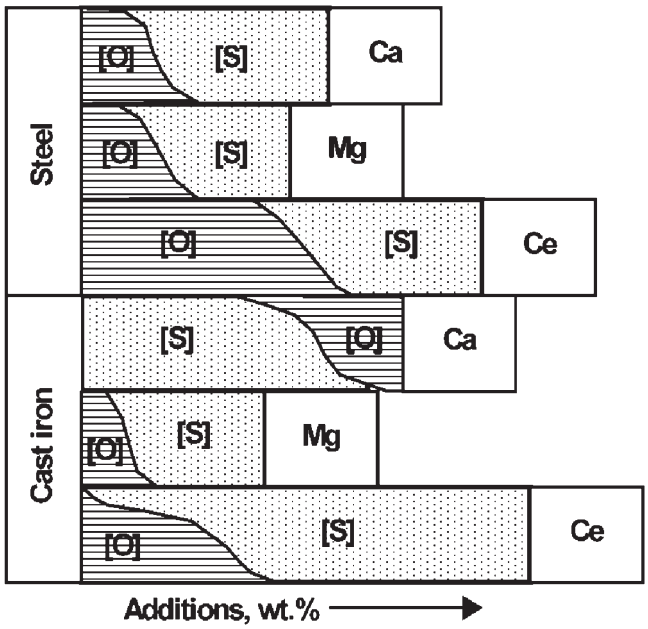

Figure 6. Sequence of the reactions of alkali and rare earth metals with impurities in the liquid steel and cast iron.

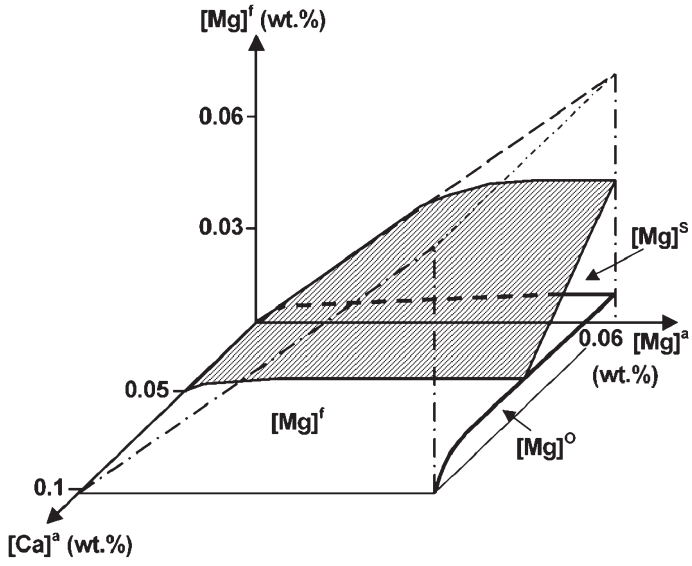

Figure 7. Interaction of Mg^a - Ca^a additives in liquid cast iron.

stable *Ca* recovery. Comparison of computed sequences of *Ca* reactions in the liquid steel with transformation of the inclusion population showed that, when *Ca* recovery was high, both de-*S* and de-*O* took place. At the same time, the real refining reactions were more complicated than those predicted by thermodynamic modeling.

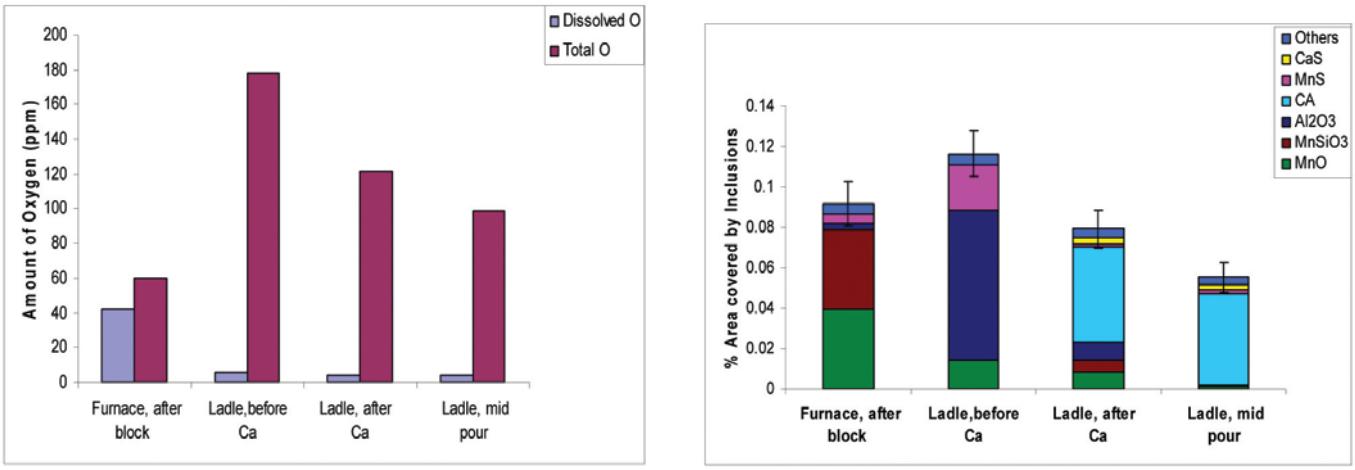

(a) *(b)*

Figure 8. (a) Dissolved and total oxygen and (b) non-metallic inclusions in steel melted in 20t EAF with acid lining and treated by Ca-wire in the ladle.[9]

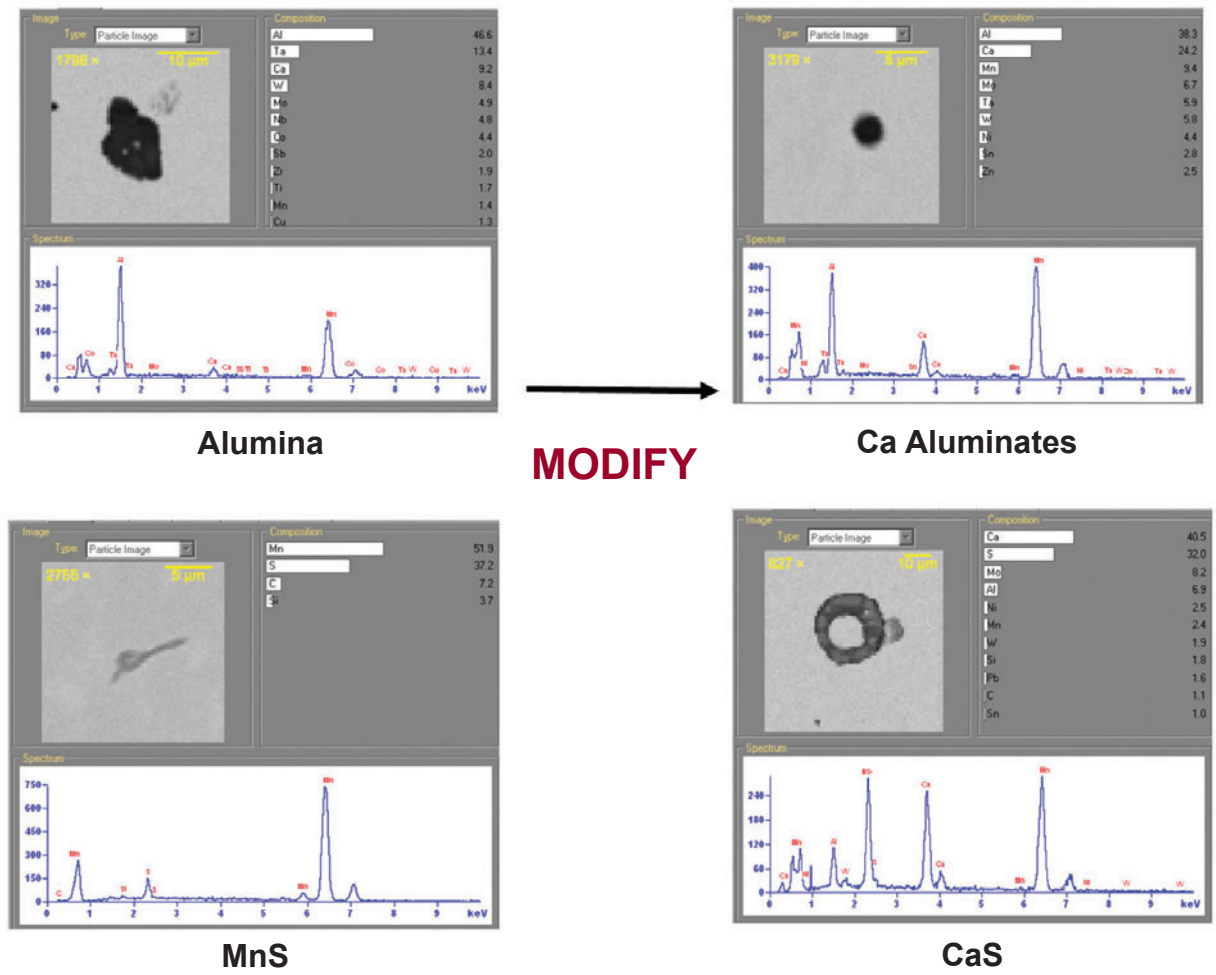

Figure 9. SEM/EDS images of alumina and MnS modification by Ca in steel.[9]

Transformation of Non-Metallic Inclusion in Di Processing

Initial Melt from Furnace

The results of inclusion measurements (2.9 mm^2 area) are given in ternary maps of the oxide and sulfide inclusions s are shown in Fig. 11. The main oxides formed were with *Si, Ti*, and *Al* while most sulfides were formed by *Mn*.

Iron Melt After Rem (*Ce+La* Mishmetal) Pre-Treatment in Furnace

Rare earth metal (REM) treatment completely changes the inclusion population and the composition in the iron melt. Two different groups of inclusions were observed with the BSED detector which is sensitive to atomic number. The first group included white *Ce-La-S* inclusions with an average 1.3 µm in diameter and an average population density of 170 mm^{-2} (Fig. 12). The second group included gray oxide and sulfide inclusions 1-3 µm in diameter containing multiple elements with an average population density of 56 mm^{-2}. Mapping of all gray inclusions containing *Ca, Mg* and *Ce* are given in Fig. 13.

Features in Di Chilled Samples (Submerged Sampler in Ladle)

Three groups of inclusions were observed and analyzed. The first group of inclusions was associated with a graphite phase. This group contained complex *Ce-La-Mg* sulfides (Fig. 14a), sometime additionally with *Ti* (Fig. 14b), *Ca-Mg-Si* oxides (Fig. 14c), and complex oxysulfides (Fig. 14d) with a total population density of 309 mm^{-2}. *Ce-Ca-Mg* mapping of all inclusions associated with the graphite phase is given in Fig. 15.

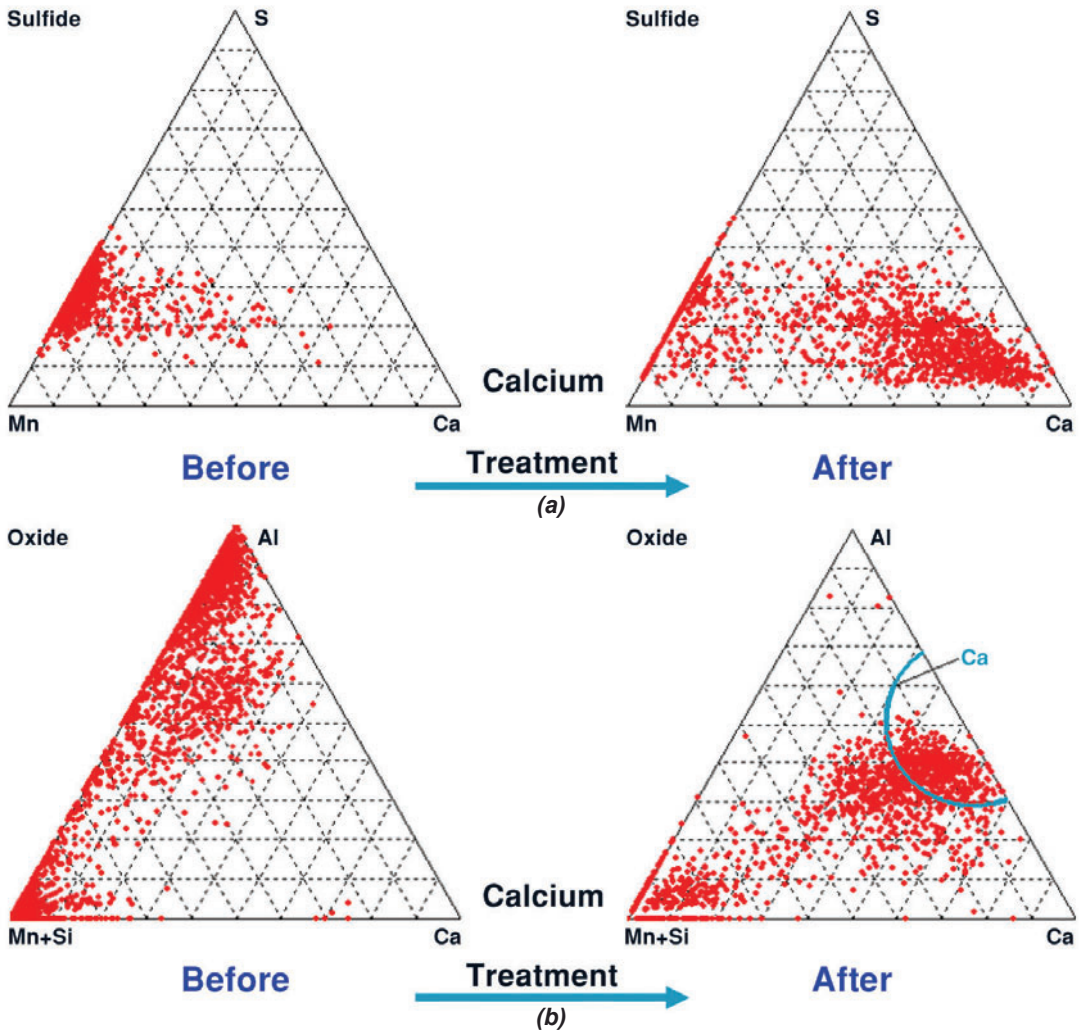

Figure 10. (a) Sulfides Mn-Ca-S and (b) oxides (Mn+Si)-Ca-Al mapping before and after addition of Ca in ladle.[10]

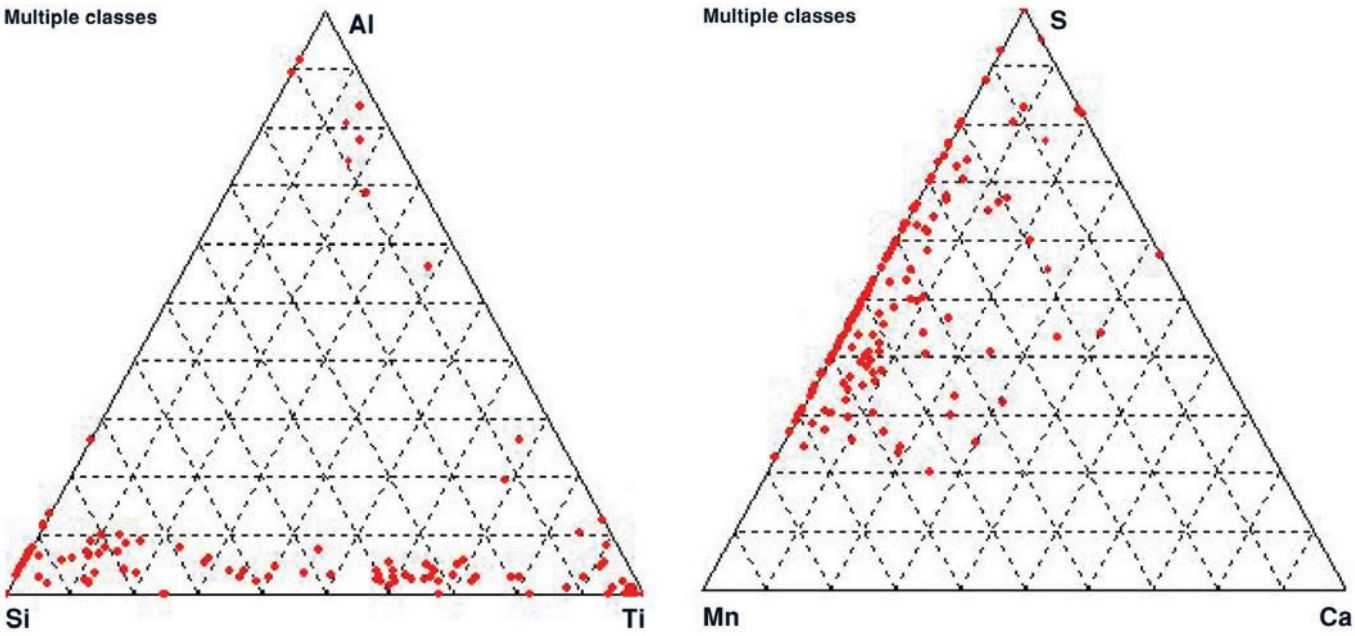

(a) *(b)*

Figure 11. Mapping of (a) Si-Ti-Al oxides and (b) Mn-Ca sulfides in initial melt.

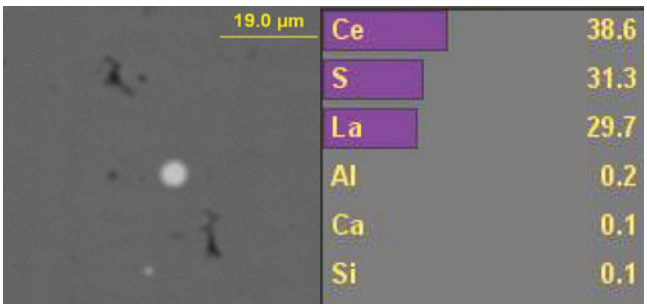

Figure 12. SEM/EDS images of REM inclusions.

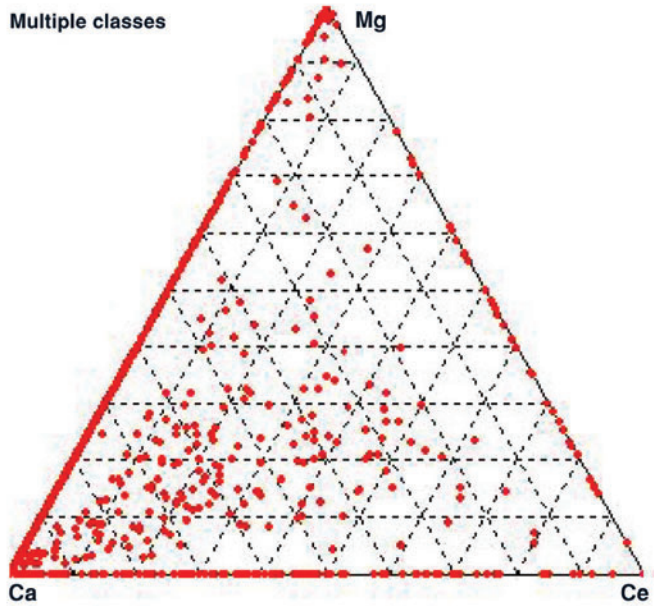

Figure 13. Mapping of Ca-Mg-Ce gray inclusions in the melt treated by REM.

The second group consisted of white inclusions in a metallic matrix with a similar composition which was observed in melt treated only with REM in the furnace. The third group contains different classes of gray inclusions with a population density of 109 mm^{-2} dispersed in the metallic matrix and not associated with the graphite phase. Compositions of these inclusions are given in Fig. 16 is a mapping of oxides and sulfides.

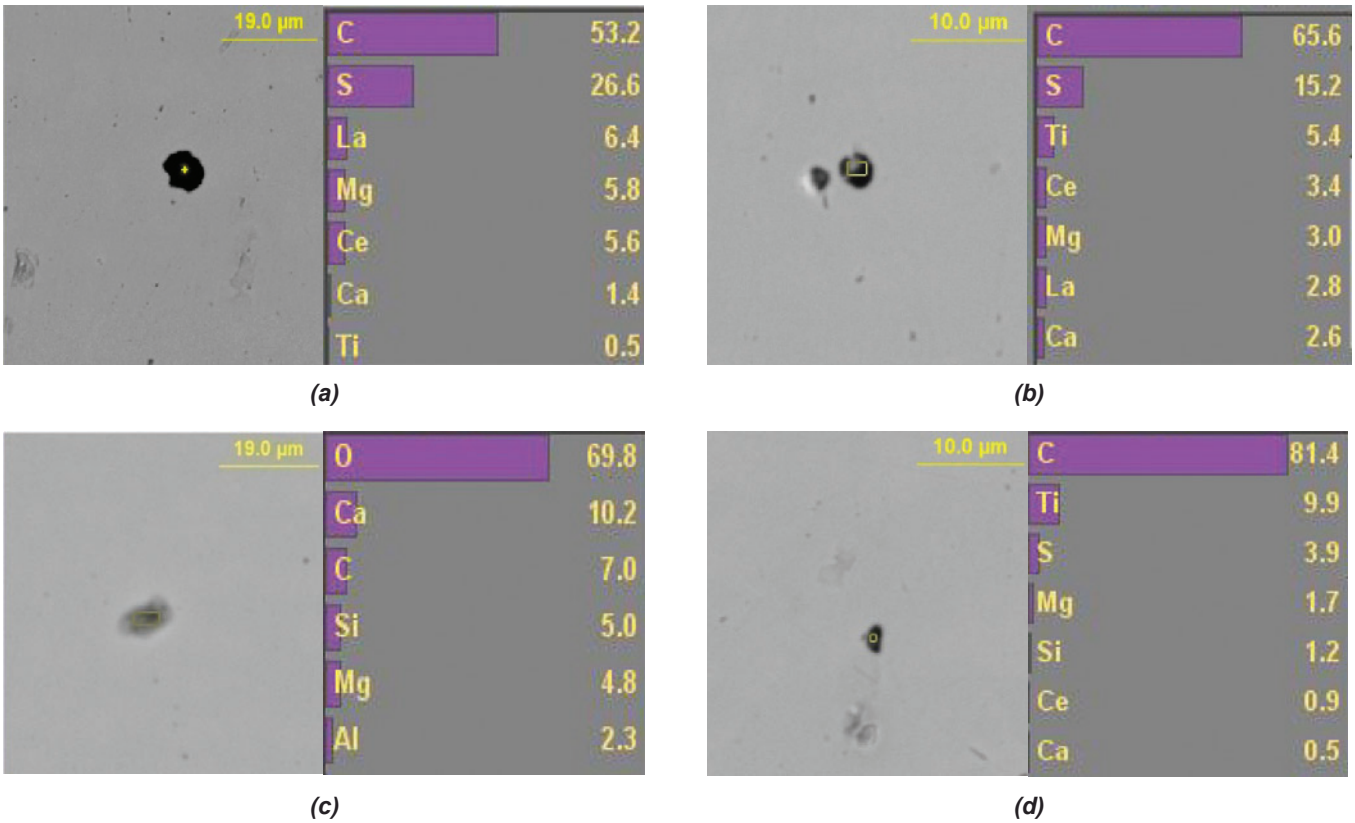

Figure 14. Different types on non-metallic inclusions associated with graphite phase in DI submerged sample.

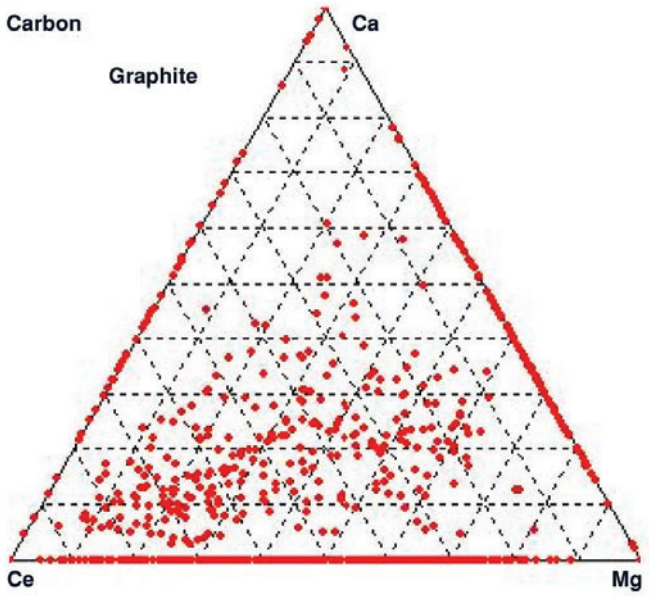

Figure 15. Mapping of Ca-Mg-Ce inclusions associated with graphite in submerged sample taken from DI in ladle.

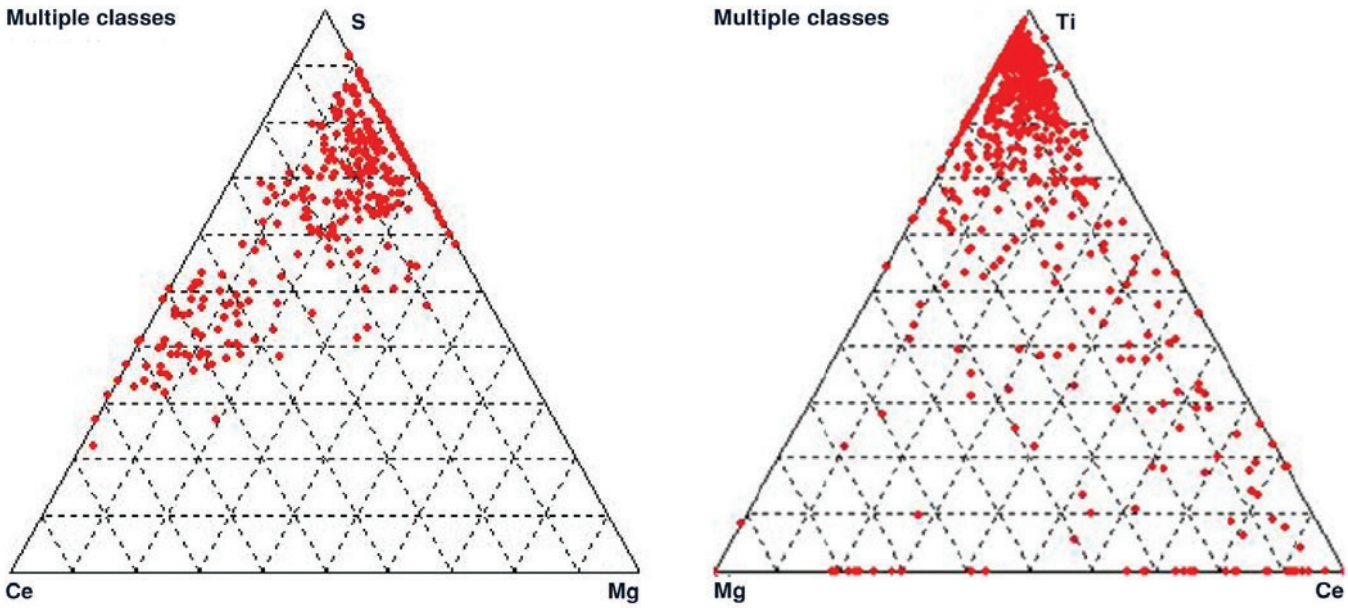

Figure 16. Mapping of (a) sulfide and (b) oxide inclusions in DI matrix and did not associated with graphite nodules (submerged sample in ladle).

Table 2. Measured Features in DI Casting.

Type	Number (mm^{-2})	Average diameter (μm)
Graphite nodules	269	11.9
REM inclusion (white)	51	0.62
Other inclusions (gray)	311	0.83

Table 3. The Possible Effects of Non-Metallic Inclusions in Steel and Iron

Alloy	Effect description	Results
Steel	Nucleate voids during fracture	Negative effect on mechanical properties
Iron	Nucleate graphite during solidification	Improve mechanical properties Decrease shrinkage Decrease chill tendency

Features in DI Casting

Three important features include graphite nodules, white REM inclusions, and gray inclusions (Table 2).

EDS analysis of graphite nodules in DI castings showed that only a small portion of the nodules had a detectable level of other elements. Fig. 17 shows mapping of these nodules. *Ce, Mg, Ca, and Si* were detected in the center of some graphite nodules. Large sizes of nodules dramatically decreased the probability of cutting heterogeneous nuclei with the plane of polish as compared to the rapidly cooled submerged sample.

The significant difference in the composition of white REM containing inclusions in the DI casting matrix were discovered (Fig. 18) when compared to samples collected directly from the melt. These white inclusions in the DI casting contained near 20%*P* and 10%*Ti*. Finally, Fig. 19 is showing the composition map of gray inclusions which were found in the metallic matrix of DI casting.

Discussion

Non-metallic inclusions formed during refining treatment could play different roles in steel and irons. The possible effects of inclusions in steel having relatively homogenous structure and in irons with highly heterogeneous structure are shown in Table 3. If cleanliness is important for achieving high impact energy in steel, some types of inclusions could improve the mechanical properties of DI casting by initiating heterogeneous graphite nucleation.

The suggested methodology provided important statistically valuable information about the composition of heterogeneous nuclei in DI. It is important to mention that direct sampling from the melt and rapid cooling of DI increased the probability of finding heterogeneous nuclei inside the small graphite nodules. In a 20 mm (2 cm) thick wall casting, less than one hundred inclusions were indicated during analysis of thousands graphite nodules. In rapid cooled samples, most of the carbon containing features were associated with different types of non-metallic inclusions.

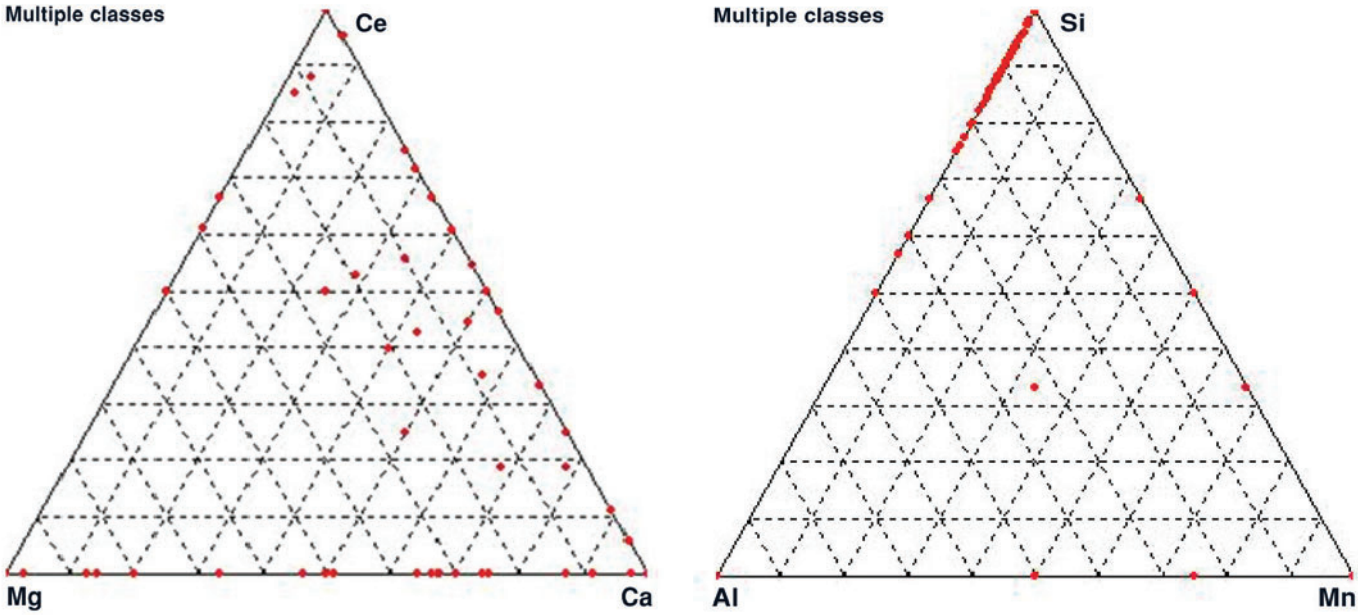

Figure 17. Mapping of inclusions found inside graphite nodules of DI casting.

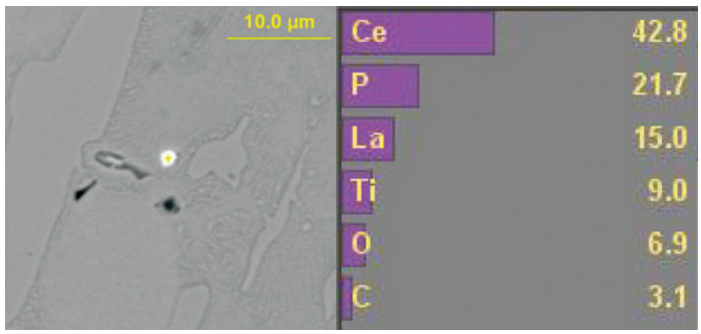

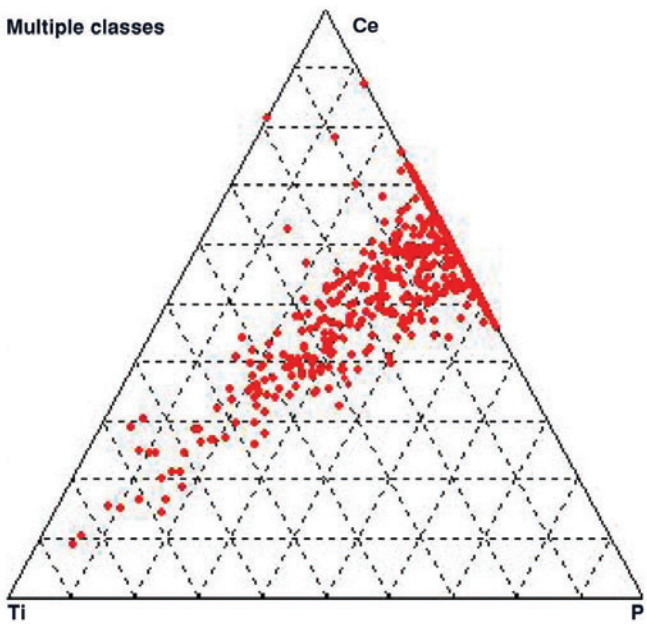

Figure 18. White REM inclusions containing phosphorus in DI casting matrix.

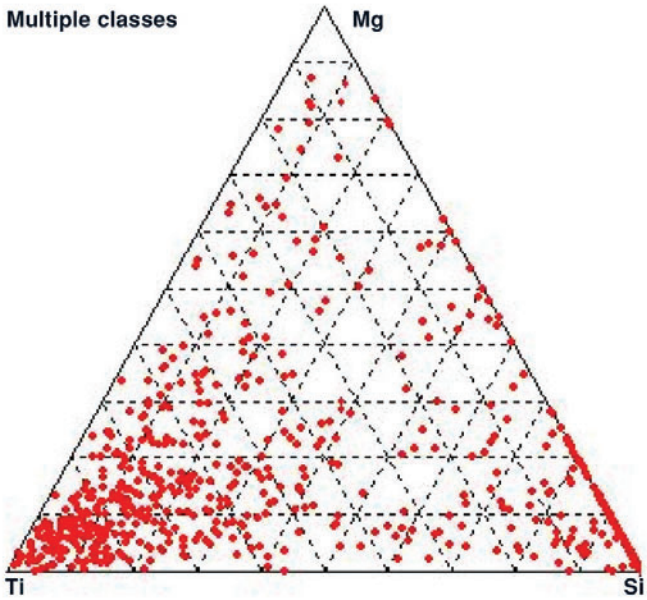

Figure 19. Mapping of all gray inclusions found in metallic matrix of DI casting.

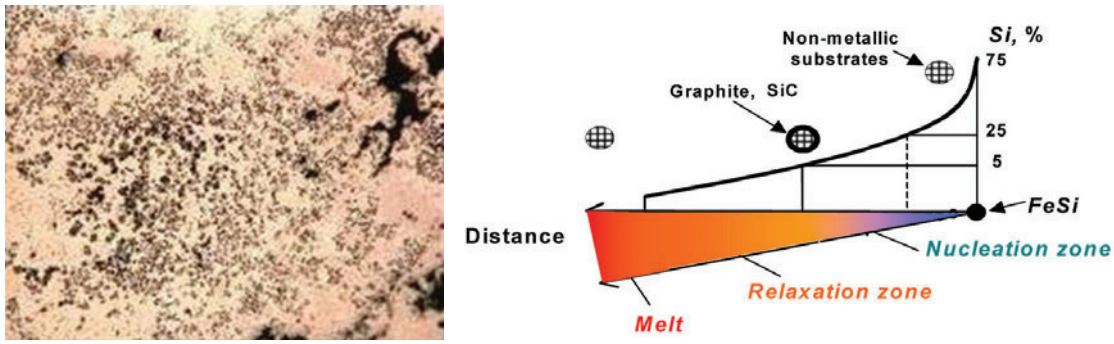

(a) ***(b)***

Figure 20. (a) Quenched supersaturated region with high density of carbon/inclusion population and (b) diagram represented dissolution zone.

Harding, Campbell, and Saunders[10] noted that although it is almost 50 years since the invention of DI, our understanding of the graphite nucleation mechanisms remains incomplete. Numerous investigations[1, 5-7] have examined the nature of the nuclei and have found that inside of the graphite spheroids there are many different chemical species, which act as effective nuclei. This study provided a broader picture of graphite heterogeneous nucleation by analyzing thousands of inclusions, classifications, and mapping.

The following question arises: "Why does such strong heterogeneous nucleation of the graphite phase take place in cast iron when compared, for example, to steel where refining of primary austenite or delta ferrite is restricted?" As was shown in this study, the population after some type of melt treatment was similar in both iron and steel. The crystal structures of these inclusions do not perfectly match atomic planes of graphite and or austenite. In addition for nucleation of graphite in cast iron there is the possibility of a local transient supersaturation effect in the vicinity of the dissolution of the FeSi carrier alloy as explained by Wang and Fredriksson[11] and Loper and coauthors.[1,3] The hypothesis is based on the experimental formation of super-saturated zones around additives dissolving in the melt, for example *FeSi* with active elements (*Mg, Ce, Ca, Ba, Al*). If the same additives were added alone, they produced significantly less effect. When the *FeSi* base particle of nodulizer or inoculant dissolves, regions in the form of roughly concentric rings with different silicon concentration will arise around the particles. The melt composition in these zones traverses from homogeneous melt to hypereutectic *Fe-C-Si* alloy, where the liquid composition is highly supersaturated and deeply under-cooled with respect to equilibrium. Thermodynamic evaluation of the carbon activity in these high silicon areas of liquid cast iron, with 2.5-3.5% carbon and at 1300-1500C (1573-1773K) temperature, allows one to calculate boundaries of primary carbon (*Si* >5-6%) and silicon carbide (*Si* >23-28%) forming. In a number of experiments, particles of primary graphite attached to non-metallic inclusions were fixed in the areas of modifier dissolution (Fig. 20).

According to this mechanism, different types of non-metallic inclusions could be activated by graphite layer precipitation in this carbon super-saturated dissolution zone. As was shown in this study, different types of sulfides and oxides were associated with graphite in the sample taken directly after DI treatment with a submerged sampler (Fig. 14 - Fig.16). These inclusions activated by graphite layers will serve as ideal heterogeneous nuclei during spherical graphite formation in the casting.

Suggested methods of inclusion measurement directly in the melt after treatment could be used together with other methods for development of a fuller understanding of the DI and CG iron processes as well as the development of novel DI processes. In particular, the combination of the suggested methods of inclusion measurement and evaluation with ATAS seem to be very promising because the inclusion characterization methods give the direct information about inclusion chemistry, size, and quantity while the thermal analysis methods will provide information about the effect of these inclusions on specific kinetic parameters reflected in the cooling curve (undercooling, rate of graphite solidification, and nodule quantity). Thermodynamic calculations will also provide valuable additions to future work allowing prediction of the reaction paths and the chemistry of reaction products.

Conclusions

Computer simulations and experiments measuring the oxygen activity and residual sulfur content were used for the determination of the sequence of the refining reactions in the iron and steel melts. These reactions have features which depend on the chemical properties of the species and also on the quality of the initial melts. Statistics of non-metallic inclusion (size, shape, composition) were studied in the iron and steel samples collected by quenching after different stages of melt treatment as well as from castings. The suggested methodology of inclusion analysis could be applied together with ATAS for solving practical problems such as decreasing shrinkage defects in ductile iron.

REFERENCES

1. Loper C. R., "Inoculation of Cast Iron – Summary of Current Understanding", AFS Transactions, vol. 107, pp 523-528 (1999).
2. Loper C. R., Winardi L., and Lekakh S., "Experiments in Pretreatment of Ductile Iron", AFS Transactions, vol. 110, pp 861-867 (2002).
3. Lekakh S. and Loper C. R., "Improving Inoculation of Ductile Iron", AFS Transactions, vol. 111, pp 885-894 (2003).
4. Lekakh S., Robertson D., and Loper C. R., "Thermochemistry and Kinetics of Iron Melt Treatment", World Foundry Congress Proceedings, UK (2006).
5. Skaland T, "Nucleation Mechanism in Ductile Iron", Proc. AFS Cast Iron Inoculation Conference, pp 13-30 (2005).
6. Igarashi Y. and Senri Okada S., "Observation and Analysis of the Nucleus of Spheroidal Graphite in Magnesium Treated Ductile Iron", Int. J. Cast Metals Res., 11, pp 83-88 (1998).
7. Riposan I., Chisamera M., Stan S. and Skaland T., "A New Approach to Graphite Nucleation Mechanism in Gray Irons", Proc. AFS Cast Iron Inoculation Conference, pp 31-41 (2005).
8. Schamber F. and Van Beek C., "Understanding Particulate Contaminates via Automated Electron Beam Analysis", Aspex Corporation (2003).
9. Singh V., Lekakh S., and Peaslee K., "Using Automated Inclusion Analysis for Casting Process Improvements". Proceedings of the Steel Founders' Society of America 62th Annual Technical and Operating Conference, Chicago (2008).
10. Harding, R.A., Campbell J., and Saunders N.J., "An Assessment of our Current Understanding of the Inoculation of Ductile Iron", International Inoculation Conference Proceedings, Rosemont, IL (1998).
11. Wang C.H. and Fredriksson H.J., "The Mechanism of Inoculation of Cast Iron Melts", Proc. 48th Int. Foundry Congress, Varna, pp 16-26 (1981).